

# Experimental estimation of distribution of excess pore pressure by cone penetration

T.G. Ha

*Posco Engineering & Construction Co., Seoul, Korea*

J.Y. Kim, J.H. Kim and C.K. Chung

*Seoul National University, Seoul, Korea*

**ABSTRACT:** This paper investigated the vertical and horizontal distribution of excess pore pressure generated by cone penetration. Multi-porous element piezocone tests were conducted in the field and physical model tests were also performed in the calibration chamber. The excess pore pressure on the cone face ( $\Delta u_1$ ) was always higher than the shoulder filter ( $\Delta u_2$ ), and  $\Delta u_1/\Delta u_2$  increased with an increase of OCR and hydrostatic pressure. The excess pore pressure decreased along the shaft as it vertically ascended from the shoulder filter, and this reduction became more significant as OCR increased. In addition, in the horizontal direction at the shoulder filter location, the excess pore pressure decreased with increasing distance from the cone in overconsolidated soils with OCR=4, whereas in heavily overconsolidated soils with OCR=10, the excess pore pressure increased from the cone boundary, reached a maximum value, and then decreased with increasing distance from the cone.

## 1 INTRODUCTION

During a piezocone penetration test (CPTu) in saturated clayey soils, excess pore pressures are generated around the cone. The induced excess pore pressures are important to evaluate geotechnical characteristics such as soil type, stress history, and undrained strength. In particular, the coefficients of consolidation and permeability are very closely related to the distribution of excess pore pressure. However, the distribution has not yet been closely clarified. Furthermore, some experimental results in overconsolidated clayey soils showed that the measured vertical and horizontal distributions were different from those employed by the theoretical dissipation models such as Torstensson, (1977), Baligh & Levadoux (1986), and Teh & Houlsby (1991).

This paper deals with the distribution of excess pore pressure induced by cone penetration in soils with a wide range of OCR. Multi-porous element piezocone tests were performed in the field to investigate the vertical distribution along the shaft. In addition, physical model tests in a calibration chamber were conducted in reconstituted kaolinite soils, where the spatial distribution of the excess pore pressure and its change with time were measured at various horizontal and vertical locations from the cone.

## 2 EXPERIMENTAL PROGRAM

### 2.1 In-situ piezocone tests

The multi-porous element piezocone is a specialized equipment for registering how the pore pressure around the cone develops and dissipates. The utilized penetrometer manufactured by A.P. van den. Berg (ELC10-5P) has a diameter of 3.57cm with an apex angle of 60°, and 5 pore pressure sensors at different positions along the shaft. Figure 1 shows the feature of the utilized multi-porous element piezocone and the filter locations ( $U_1 \sim U_5$ ).

The multi-porous element piezocone tests (MCPTu) were conducted at Incheon, Pusan, and Kimhae in the seaside districts of the Korean peninsula, where there are thick soft clayey layers. The geotechnical information of each clayey layer is presented in Table 1. Incheon has lightly overconsolidated clayey silt with  $OCR=1.5$ , while Pusan and Kimhae have normally consolidated silty clay with  $OCR=1.0$ .

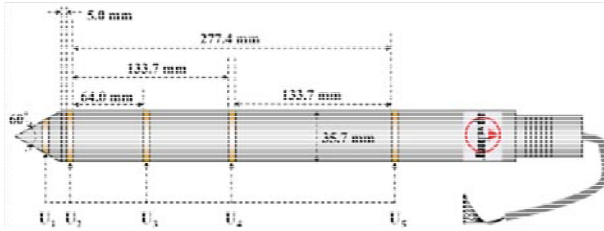


Figure 1. Multi-porous element piezocone (ELC10-5p)

Table 1. Geotechnical information of clayey layer at test sites

	Incheon	Pusan	Kimhae
Thickness of clayey layer	10.6m	44.5m	18.8m
Unified soil classification system (USCS)	ML	CL	CL
Liquid limit ( $LL$ )	31.6%	57.9%	40.5%
Plasticity index ( $PI$ )	9.2%	24.0%	11.2%
Water content ( $w_n$ )	28.5%	40.7%	32.0%
Overconsolidation ratio ( $OCR$ )	1.5	1.0	1.0
Compression index ( $C_c$ )	0.39	0.75	0.43
Vertical coefficient of consolidation ( $c_v$ )	$4.1 \times 10^{-3} \text{ cm}^2/\text{s}$	$1.4 \times 10^{-3} \text{ cm}^2/\text{s}$	$1.2 \times 10^{-3} \text{ cm}^2/\text{s}$

### 2.2 Physical model tests in calibration chamber

#### 2.2.1 Calibration chamber system

The calibration chamber is a large model box used to simulate the in-situ stress conditions of the ground by enforcing the confining stress to the soils inside the box. In the physical model test in a calibration chamber, a homogeneous and reproducible soil specimen subjected to a known stress history can be prepared and tested under a controlled boundary condition.

The calibration chamber system used in this study is shown in Figure 2. The size of the chamber is 360 mm in inner diameter and 970 mm in height. The chamber and loading plate are made of rigid stainless steel, thus the specimen is basically consolidated in the equal strain and  $K_0$  condition. Air pressure supplied by a compressor was applied to the diaphragm to load the specimen. Pore-water was drained at the top and bottom of the specimen during the loading. The cone was pushed into the middle of

the specimen by the penetrating device mounted on the cap of the chamber. Pore pressures were measured both on the piezocone and inside the specimen. The multi-porous element piezocone in Figure 1 was utilized. The piezometers were inserted into the model ground through the chamber base at various horizontal and vertical locations, as illustrated in Figure 2a. The piezometer consists of a pore pressure transducer, an adapter, a duct, and a textile filter. The duct is a stainless steel needle with an inside diameter of 1.0 mm and a thickness of 0.3 mm. The tips of the ducts were sealed with a filter material, in order to prevent clogging of the tubes due to soil migration. A more detailed description of the chamber system is given by Ha (2009).

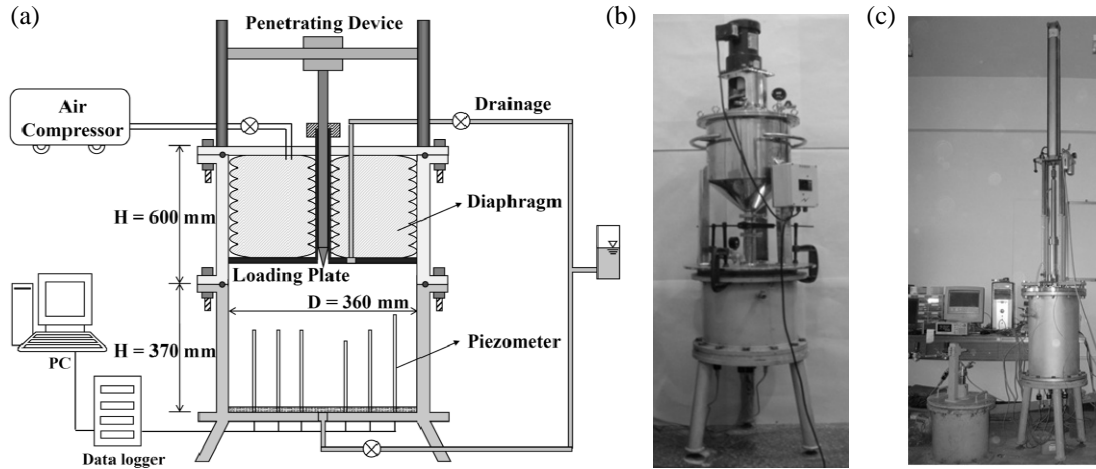


Figure 2. Calibration chamber system: (a) Schematic diagram, (b) Mixing chamber, (c) Assembled calibration chamber system

### 2.2.2 Geotechnical characteristics of specimen

Kaolinite is a clay mineral with the characteristics of low plasticity and low compressibility. Pure and homogeneous EPK kaolinite was used to make a model ground. The engineering properties of model ground soil are presented in Table 2. The coefficients of consolidation in vertical ( $c_v$ ) and horizontal ( $c_h$ ) directions were obtained from the oedometer tests. Average values of  $c_v$  and  $c_h$  in the normally consolidated (NC) state are  $0.5 \times 10^{-3} \text{ cm}^2/\text{s}$  and  $1 \times 10^{-3} \text{ cm}^2/\text{s}$ , respectively, whereas those in the overconsolidated (OC) range with  $1.7 \leq \text{OCR} \leq 3.3$  are  $2 \times 10^{-3} \text{ cm}^2/\text{s}$  and  $4 \times 10^{-3} \text{ cm}^2/\text{s}$ .

Table 2. Engineering properties of soil specimen

Property		Value
Liquid limit ( $LL$ )		53%
Plasticity index ( $PI$ )		20%
Percent finer than No. 200 sieve		98%
Vertical coefficient of consolidation ( $c_v$ )	NC	$0.3\text{--}0.7 (\times 10^{-3} \text{ cm}^2/\text{s})$
	OC	$1.0\text{--}3.0 (\times 10^{-3} \text{ cm}^2/\text{s})$
Horizontal coefficient of consolidation ( $c_h$ )	NC	$0.8\text{--}1.2 (\times 10^{-3} \text{ cm}^2/\text{s})$
	OC	$3.0\text{--}5.0 (\times 10^{-3} \text{ cm}^2/\text{s})$

### 2.2.3 Test procedure

A homogenous and fully saturated model ground was made using the mixing chamber in Figure 2b. Kaolinite powder was mixed into slurry at a water content of two

times higher than the liquid limit. The slurry was mechanically blended with a spinning blade and vacuum pressure was applied to extract the air from the slurry. After removing the air, the slurry was carefully poured into the testing chamber. Following the sedimentation of the slurry and the consolidation under a small dead-weight (3kPa), the chamber system was assembled as shown in Figure 2c. To acquire the rigorous pore pressure data, the porous filters of piezocone and the piezometers were completely saturated with glycerin in the vacuum chamber. Then, the pressure was incrementally applied. The settlement of the specimen, water discharge and pore pressures were monitored to identify the end of consolidation. After completing the consolidation, the piezocone was pushed into the specimen at the rate of 2 cm/s by the penetrating device. Once the piezocone reached the desired depth, the penetration was stopped and the dissipation test had been conducted for a sufficient length of time. The response of the excess pore pressure during the penetration and dissipation was measured every 1.0 sec on the piezocone and inside the model ground using the data acquisition system.

#### 2.2.4 Test program

Four sets of the physical model test in the calibration chamber were conducted, as summarized in Table 3. The values of OCR were set as 1, 4 and 10 to verify the effect of stress history on the excess pore pressure distribution by cone penetration. Meanwhile, the hydrostatic pressure ( $u_0$ ) can also affect the distribution, as discussed in Sully et al. (1988). However, the value of  $u_0$  in the physical model test is inevitably very low because of the limited height of the specimen. Accordingly, the artificial pseudo-hydrostatic pressure was enforced in Test III and Test IV by applying additional pressure under an undrained condition. These values were set to be equal to the effective vertical stress ( $\sigma'_{v0}$ ) of the test. As seen in Table 3, the only difference in the condition between Test II and Test III is the value of  $u_0$ .

Table 3. Program, summary, and results of physical model tests

		Test I	Test II	Test III	Test IV
Program	OCR	1	4	4	10
	$\sigma'_{v0}$ (kPa)	50	20	20	10
	$u_0$ (kPa)	1	2	20	10
Summary	Consolidation time (day)	30	60	60	60
	Height of specimen (cm)	24	32	32	32
	Penetration depth (cm)	14	22	22	22
Result	$\Delta u_1/\Delta u_2$	1.04	1.09	1.80	3.20

### 3 EXCESS PORE PRESSURE DISTRIBUTION DUE TO CONE PENETRATION

#### 3.1 Vertical distribution of excess pore pressure

The vertical distribution of excess pore pressure along the penetrometer during the cone penetration was estimated from MCPTu both in the field and in the calibration chamber. Figure 3 shows the differences of pore pressure ( $u_1-u_2$ ) between the cone face and the shoulder filter locations ( $U_1$  and  $U_2$ , respectively), using the OCR-PPD monograph proposed by Sully et al. (1988). The Pore Pressure Difference (PPD), defined as Equation 1, increases as the OCR increases, and the results coincide well with the correlation in Equation 2 suggested by Sully et al. (1988).

$$PPD = \frac{u_1 - u_2}{u_0} \quad (1)$$

$$OCR = 0.66 + 1.43PPD \quad (2)$$

The ratio of the excess pore pressure at the cone face to that of the shoulder filter ( $\Delta u_1/\Delta u_2$ ) is derived as Equation 3 from Equation 1 and Equation 2.

$$\frac{\Delta u_1}{\Delta u_2} = \frac{u_1 - u_0}{u_2 - u_0} = 1 + \frac{OCR - 0.66}{1.43\Delta u_2} u_0 \quad (3)$$

It can be estimated from Equation 3 that the excess pore pressure on the cone face ( $\Delta u_1$ ) is always higher than that of the shoulder filter ( $\Delta u_2$ ), and the ratio,  $\Delta u_1/\Delta u_2$ , increases with an increase of OCR and  $u_0$ . Results of physical model tests in Table 3 support the above hypothesis. In particular, despite the same stress history (OCR = 4),  $\Delta u_1/\Delta u_2 = 1.09$  was measured in Test II while  $\Delta u_1/\Delta u_2 = 1.80$  was recorded in Test III. This variation arises from the difference in the hydrostatic pressure between the tests.

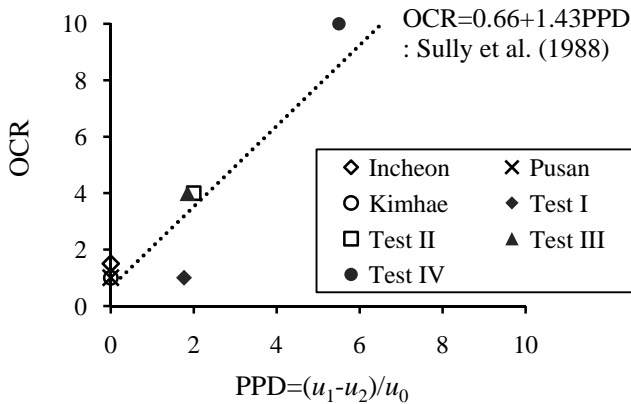


Figure 3. Relationship between PPD and OCR

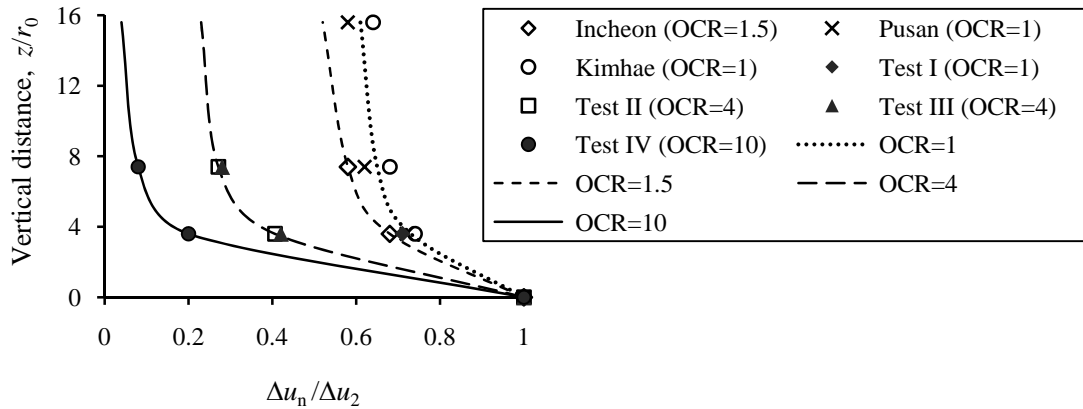


Figure 4. Estimated vertical distribution of excess pore pressure along the shaft

Figure 4 shows the vertical distribution along the shaft with varying OCR values. Penetration-induced excess pore pressures at the shaft ( $U_3$ – $U_5$ ) normalized by the value at the shoulder filter, for example,  $\Delta u_3/\Delta u_2$ ,  $\Delta u_4/\Delta u_2$ , and  $\Delta u_5/\Delta u_2$  are plotted in terms of the vertical distance from the shoulder filter normalized by the cone radius ( $z/r_0$ ). It can be seen that the excess pore pressure decreases as it ascends from the shoulder filter, i.e.  $\Delta u_2 > \Delta u_3 > \Delta u_4 > \Delta u_5$ . In addition, the excess pore pressure ratio decreases more rapidly as OCR increases. Meanwhile, the similar vertical distributions were measured in Test II (OCR=4) and Test III (OCR=4), which means that  $u_0$  has little influence on the vertical distribution along the shaft. The fitting curves for each OCR have been proposed in the figure. From the interpolation technique applied to these curves, we can approximately estimate the vertical distribution along the shaft according to the value of OCR.

### 3.2 Horizontal distribution of excess pore pressure

Figure 5 presents the horizontal distribution of excess pore pressure in the soil at the shoulder filter location measured by piezometers in the calibration chamber. The excess pore pressures normalized by the value of the shoulder filter at  $r = r_0$  are plotted against the normalized radial distance from the center of the cone ( $r/r_0$ ). Unfortunately, the appropriate data were not acquired from Test I (OCR = 1) because of the clogging of the duct and the pressure leakage on the adapter.

As can be seen from the results of Test II and Test III in Figure 5a, the excess pore pressure in soils with OCR = 4 is maximum at the shoulder filter location and decreases logarithmically with an increase in distance, as suggested by Torstensson, (1977), Baligh & Levadoux (1986), and Teh & Houlsby (1991). The horizontal distribution is little affected by  $u_0$ . However, in heavily overconsolidated soils with OCR = 10, the excess pore pressure increases from the cone boundary and reaches a maximum value of  $1.12\Delta u_2$  around  $r = 2r_0$  and then decreases as the distance from the cone increases, as shown in Figure 5b.

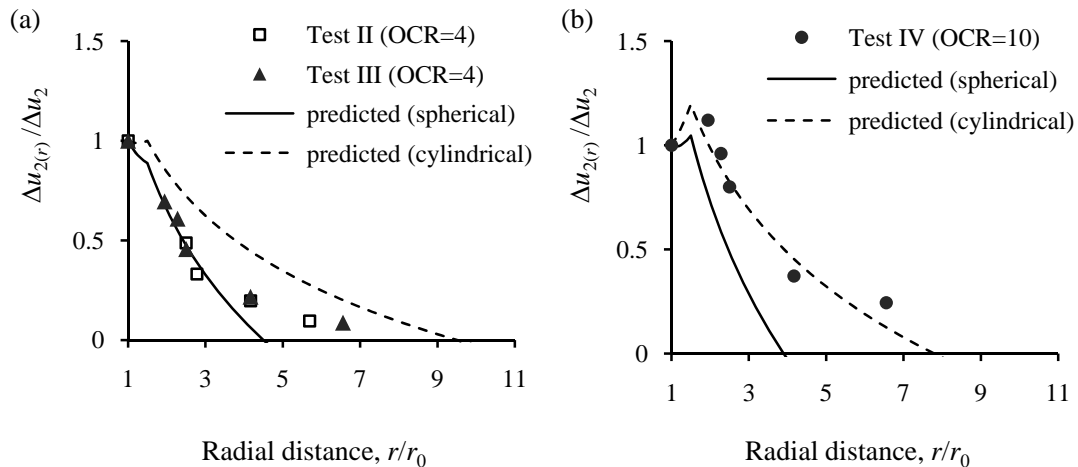


Figure 5. Estimated horizontal distribution of excess pore pressure at the shoulder filter location from in-situ tests and physical model tests in the calibration chamber: (a) OCR=4, (b) OCR=10

The horizontal distribution can be evaluated with a theoretical framework based on the cavity expansion theory and the critical state soil mechanics suggested by Burns & Mayne (1998). The excess pore pressure at the shoulder filter location ( $\Delta u_2$ ) is the sum of that induced by the octahedral normal stress ( $\Delta u_{2oct}$ ) in Equation 4 and that induced by the octahedral shear stress ( $\Delta u_{2shear}$ ) in Equation 5.

$$\Delta u_{2oct} = \frac{4}{3} s_u \ln I_r \quad (4)$$

$$\Delta u_{2shear} = \sigma'_{v0} \left[ 1 - \left( \frac{OCR}{2} \right)^\Lambda \right] \quad (5)$$

where  $s_u$  is the undrained shear strength,  $I_r$  is the rigidity index ( $I_r = G_{50}/s_u$ ,  $G_{50}$  is the secant shear modulus at 50% of failure stress), and  $\Lambda$  is the plastic volumetric strain ratio ( $\Lambda = 1 - C_c/C_s$ ,  $C_s$  is the swelling index, and  $C_c$  is the compression index).  $\Delta u_{2oct}$  is assumed to decrease logarithmically in accordance with the distance from the cone within the plastic zone. The radius of the plastic zone ( $r_p$ ) can be determined from the spherical or cylindrical cavity expansion theory in Equation 6 and Equation 7.  $\Delta u_{2shear}$  is considered to vary linearly within the shear zone ( $r_s$ ).

$$r_p = r_0 I_r^{1/3} \quad : \quad \text{Spherical cavity expansion theory} \quad (6)$$

$$r_p = r_0 I_r^{1/2} \quad : \quad \text{Cylindrical cavity expansion theory} \quad (7)$$

Table 4 provides the components required to evaluate the horizontal distribution from the shoulder filter location. The values of  $s_u$  and  $I_r$  were obtained from  $K_0$ -consolidated, undrained triaxial compression tests (CK<sub>0</sub>U TXC) performed under the stress state identical to the corresponding physical model test. The value for  $\Lambda$  of the specimen was determined from the oedometer tests. The values of  $r_p$ ,  $\Delta u_{2oct}$ , and  $\Delta u_{2shear}$  were calculated from Equations 4~7, whereas  $r_s = 1.5r_0$ , i.e. the size of the shear zone is 9mm, was determined based on the suggestion ( $r_s = 1.1r_0 \sim 1.6r_0$ ) by Burns & Mayne (1998) and the experimental estimations ( $r_s = 1.5r_0 \sim 1.8r_0$ ) by Kim et al. (2007).

The evaluated horizontal distributions are shown in Figure 5. It can be seen that the selected  $r_s = 1.5r_0$  provides a good prediction for Test IV. The measured data in Test II & Test III with OCR=4 exist between the predictions by the spherical and the cylindrical cavity expansion theory. Meanwhile, for Test IV with OCR=10,  $r_p$  computed by the cylindrical cavity expansion theory offers a more appropriate prediction than the spherical cavity expansion theory. These results coincide with the opinion of Burns & Mayne (1998) in that the zone surrounding the shoulder filter is neither completely spherical nor cylindrical, but represents a transitional area between the two shapes.

Table 4. Component to evaluate the horizontal distribution

	OCR	$\sigma'_{v0}$ (kPa)	$s_u$ (kPa)	$I_r$	$\Lambda$	$r_s/r_0$ (assumed)	$r_p/r_0$		$\Delta u_{2oct}$ (kPa)	$\Delta u_{2shear}$ (kPa)
							Spherical	Cylindrical		
Test II & Test III	4	20	13.9	90	0.8	1.5	4.5	9.5	83	-15
Test IV	10	10	14.5	61	0.8	1.5	3.9	7.8	79	-26

## 4 SUMMARY AND CONCLUSIONS

The spatial distributions of excess pore pressure generated by cone penetration were experimentally estimated with various OCR values through in-situ tests and physical model tests in the calibration chamber. Comparing the estimated distributions with the theoretical suggestions and the previous experimental results, the following conclusions have been drawn.

(1) The excess pore pressure on the cone face ( $\Delta u_1$ ) is always higher than the shoulder filter ( $\Delta u_2$ ). And, the ratio,  $\Delta u_1/\Delta u_2$ , increases as OCR and the hydrostatic pressure ( $u_0$ ) increase.

(2) In the vertical direction along the shaft, the excess pore pressure decreases as it ascends from the shoulder filter. In addition, in soils with a higher OCR, the excess pore pressure decreased more rapidly.

(3) In the horizontal direction at the shoulder filter location, the excess pore pressure decreases logarithmically in accordance with the distance from the cone body in overconsolidated clayey soils with OCR=4, whereas the excess pore pressure increases from the cone boundary, reaches the maximum value, and then decreases logarithmically in heavily overconsolidated clayey soils with OCR=10.

## 5 ACKNOWLEDGEMENTS

This research was supported by SNU SIR Group of the BK21 research Program funded by Ministry of Education & Human Resources Development and Expressway & Transportation Research Institute of Korea Expressway Corporation.

## 6 REFERENCES

- Baligh, M.M. & Levadoux, J.M. 1986. Consolidation after undrained piezocone penetration II: interpretation. *Journal of Geotechnical Engineering, ASCE* 112(7): 727-745.
- Burns, S.E. & Mayne, P.W. 1998. Monotonic and dilatatory pore-pressure decay during piezocone tests in clay. *Canadian Geotechnical Journal* 35: 1063-1073.
- Ha, T.G. (2009). Piezocone dilatatory dissipation model for evaluation of coefficient of consolidation in overconsolidated clayey soils. Ph. D. Dissertation, Seoul National University, Seoul, Korea.
- Kim, T.J., Kim, N.K., Tumay, M.T., and Lee, W.J. 2007. Spatial distribution of excess pore-water pressure due to piezocone penetration in overconsolidated clay. *Journal of Geotechnical and Geoenvironmental Engineering, ASCE* 133(6): 674-683.
- Sully, J.P., Campanella, R.G., and Robertson, P.K. 1988. Overconsolidation ratio of clays from penetration pore water pressures. *Journal of Geotechnical Engineering, ASCE* 114(2): 209-215.
- Teh, C.I. & Houlsby, G.T. 1991. An analytical study of the cone penetration test in clay. *Geotechnique* 41(1): pp. 17-34.
- Torstensson, B.A. 1977. The pore pressure probe. *Nordiske Geotekniske Mte, Oslo*. Paper 34: 34.1-34.15.